Quantitative Performance Assessments for Neuromagnetic Imaging Systems

Ryo Koga, Ei Hiyama, Takuya Matsumoto, and Kensuke Sekihara, *Fellow IEEE*

Abstract— We have developed a Monte-Carlo simulation method to assess the performance of neuromagnetic imaging systems using two kinds of performance metrics: A-prime metric and spatial resolution. We compute these performance metrics for virtual sensor systems having 80, 160, 320, and 640 sensors, and discuss how the system performance is improved, depending on the number of sensors. We also compute these metrics for existing whole-head MEG systems, MEGvision^{TM} (Yokogawa Electric Corporation, Tokyo, Japan) that uses axial-gradiometer sensors, and TRIUX^{TM} (Elekta Corporate, Stockholm, Sweden) that uses planar-gradiometer and magnetometer sensors. We discuss performance comparisons between these significantly different systems.

I. INTRODUCTION

Electrophysiological activity of neurons in the cerebral cortex generates tiny magnetic fields outside the scalp. Direct non-invasive measurements of these neuronal activities in the sub-millisecond time scale can be achieved with magnetoencephalography (MEG)[1]. Modern MEG systems are capable of whole-head coverage with simultaneous measurements of more than 300 sensors. Such whole-head sensor arrays, together with advanced signal processing algorithms, now enable imaging of dynamic brain activity – referred to as neuromagnetic imaging[2][3].

We have developed a Monte-Carlo simulation method to assess the performance of neuromagnetic imaging systems. The method uses two kinds of performance metrics based on the signal-detection theory: A-prime metric and spatial resolution. The A-prime metric represents imaging system's ability to detect multiple sources, and the spatial resolution expresses system's ability to discriminate closely-located two sources.

Since these performance metrics depend on the locations and orientations of sources, Monte-Carlo computer simulation is needed in which these metrics are computed using a large number of Monte-Carlo trials, each trial having random source locations and orientations. A similar Monte-Carlo simulation method was previously used for comparing performances of imaging algorithms[4]. In this paper, performances of various types of sensor hardware are compared, with the imaging algorithm being fixed to the adaptive beamformer algorithm[3][5], which is one of representative algorithms in neuromagnetic imaging.

We compute these performance metrics for virtual sensor systems having 80, 160, 320, and 640 sensors, and discuss

Authors are with the Department of Systems Design and Engineering, Tokyo Metropolitan University, Asahigaoka 6-6, Hino, Tokyo 191-0065, Japan.
K. Sekihara is a corresponding author ksekiha@sd.tmu.ac.jp.

how the system performance is improved, depending on the number of sensors. We also compute these metrics for existing whole-head MEG systems, and compare their performances.

II. MONTE CARLO COMPUTER SIMULATION

A. Sensor Data Generation

In our Monte-Carlo computer simulation scheme, assuming a sensor array geometry of which performance is to be tested, the simulated sensor data are computed. Here, we assume dipole sources with fixed orientations, and a two orientation forward lead field is calculated using a single spherical-shell model[6]. The source activity is projected, through the lead field, to the sensor space to create signal magnetic field. The Gaussian white noise with its standard deviation equal to 50 fT is added to this signal magnetic field to finally generate the simulated sensor data.

Multiple sources having a equal intensity are assumed, and their locations are chosen randomly within the simulated brain region in Fig. 1. As depicted in this figure, the center of the brain region is 10.5 cm below the sensor located at the center of the sensor array. A spherical region with the outer radius of 8cm and the inner radius of 1cm is defined as the brain region where the region more than 4cm below the sphere center is excluded. One hundred Monte Carlo trials
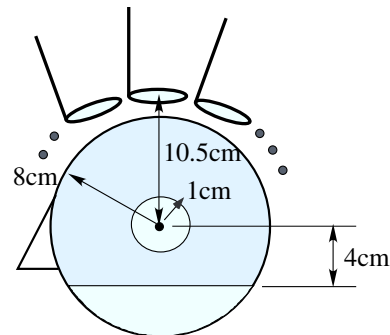

Fig. 1. Simulated brain region assumed for Monte Carlo computer simulation.

of simulated sensor data are generated, each with random source locations and orientations.

B. Source Reconstruction and Local Peak Detection

The simulated brain region in Fig. 1 is segmented into 0.5-cm voxels. Adaptive beamformer source reconstruction[3][5] is performed and a source power map (the power of the time courses at each voxel) is reconstructed at all voxel

locations. The localization accuracy is assessed in the following manner. (1) If a voxel has a value higher than its nearest three-dimensional neighbors, we determine that a local peak exists at that voxel. (2) After all the local peak locations are obtained, we test whether each local peak is within a particular distance (d) from a true source location. If a particular peak is within d from a true source location, that source is labeled as a "detected source". If there is no true source within d from the local peak, that local peak is labeled as a "false detection". In this computer simulation d is set at 0.75 cm ($1.5\times$voxel size).

C. A-prime Metric

To derive the A-prime metric, we compute the hit rate H, which is the ratio of the correct source detection. Let us define the numbers of detected sources n_D and that of undetected sources n_U. Noting that the relationship $n_D + n_U = n_T$ where n_T is the total number of true sources, the hit rate H is computed using

$$H = \left\langle \frac{n_D}{n_D + n_U} \right\rangle = \frac{\langle n_D \rangle}{n_T}, \qquad (1)$$

where $\langle \cdot \rangle$ indicate the averaging across Monte Carlo trials. Defining the number of false detections in each Monte Carlo trial as n_F, we compute the false-detection rate F using

$$F = \left\langle \frac{n_F}{n_D + n_F} \right\rangle = \left\langle \frac{n_F}{n_L} \right\rangle, \qquad (2)$$

where and n_L is the number of total local peaks in each Monte Carlo trial, and the relationship $n_L = n_D + n_F$ is used. Note that the definition of the false-detection rate above differs from that used in [4][1].

Once H and F are obtained, we can compute A-prime metric, A_p, which is equal to the area under the ROC curve for a pair of H and F[7]. The A-prime metric is given, as the first order approximation, by[2]

$$A_p = \frac{H - F}{2} + \frac{1}{2}. \qquad (3)$$

We can obtain the plot of the A-prime metric with respect to source intensity by repeating the procedure described above with different source intensities. The resultant A-prime plot expresses an ability of a given neuromagnetic imaging system to detect multiple sources with different intensities.

D. Spatial Resolution

To compute spatial resolution, we assume two sources having a, equal intensity with a fixed inter-source distance Δ, and examine the minimum distance in which the two sources can be detected. The locations and orientations of the two sources are randomly chosen in each Monte-Carlo trial, and the A-prime metric is obtained using exactly the same procedure described above. Here, the voxel size is set at 0.2Δ when $\Delta \le 2.5$ cm, and it is fixed to 0.5 cm when $\Delta > 2.5$ cm. The source-detection length d is set

---

[1] In [4], F is obtained using $F = n_F/$(maximum number of n_F). The resultant F becomes significantly different from that by Eq. (2).

[2] The second order approximation for computing A-prime is given in [7].

at $1.5\times$(voxel size), as mentioned previously. We repeat the Monte Carlo simulation with different inter-source distances, and obtain the plot of the A-prime metric versus the inter-source distance. We then look for the source distance that gives the A-prime metric equal to a certain value α ($0.5 \le \alpha \le 1$), and define this value of the source distance to be the spatial resolution of the imaging system for a given source intensity. By repeating the whole procedure with various source intensities, we obtain the plot of resolution versus the intensity of the sources, the plot representing the spatial resolution of the imaging system under assessment.

III. RESULTS OF COMPUTING PERFORMANCE METRICS
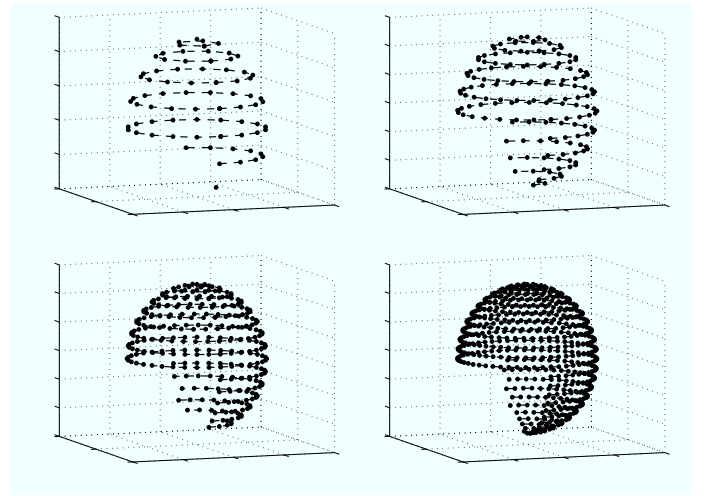
A. Assumed Sensor Systems

Fig. 2. Virtual sensor arrays assumed in computer simulation. The top-left, top-right, bottom-left, and bottom-right panels respectively show sensor systems with 80, 160, 320, and 614 sensors. Sensors are aligned on a sphere with 13 cm radius.

We assessed performances of four types of sensor systems having 80, 160, 320, and 614 sensors. The sensors are aligned on a surface of a sphere. We assume two kinds of spheres: one having a 10 cm radius and the other having a 13 cm radius. The sensor locations of the systems with the 13 cm radius are shown in Fig. 2. As shown in this figure, three quoters of the sphere surface are covered by sensors and the sensors are aligned with an equal inter-sensor spacing. The sensor is assumed to be a first-order axial gradiometer with a 5-cm baseline.

B. Ability of Detecting Multiple Sources

Plots of the hit rate, the false detection rate, and the A-prime metric with respect to source intensity were obtained for the system with 160 sensors aligned on a sphere of a 13 cm radius. We assumed that the number of sources was three. The results are presented in Fig. 3. Here the error bars indicate the range of ± 1 standard deviation. In this figure, clear tendencies can be observed in which the hit rate increases and the false-detection rate decreases as the source
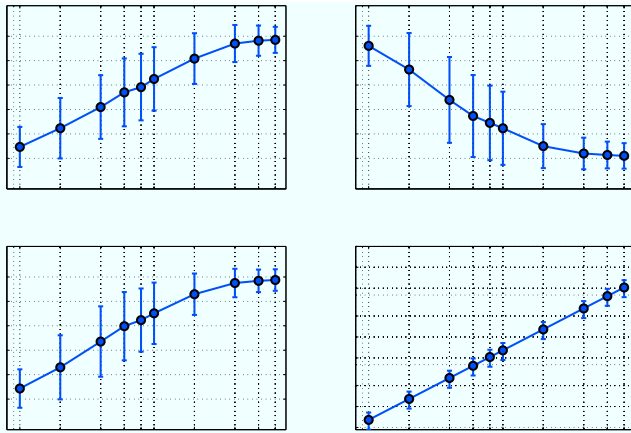
Fig. 3. (a) Plots of the hit rate, (b) the false detection rate, and (c) the A-prime metric with respect to the source intensity for the system with 160 sensors aligned on a sphere of a 13 cm radius. (d) Plot of SNR of the sensor data with respect to the source intensity. The number of sources was assumed to be three, and the sensor noise standard deviation is assumed to be 50 fT.
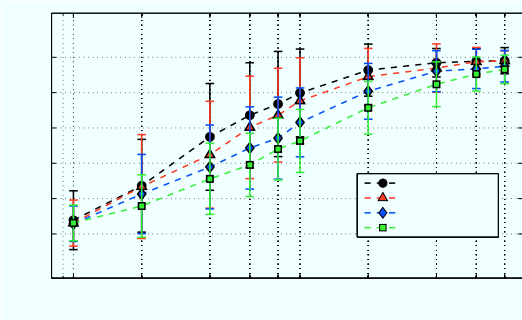

Fig. 4. A-prime metric versus source intensity for four different number of sources. The system with 160 sensors aligned on a sphere of a 13 cm radius was used.

intensity increases. Therefore, the A-prime metric increases as source intensity increases. The relationship between the source intensity and the signal-to-noise ratio (SNR) for the sensor system with a 13 cm sphere radius and for a three-source case is shown in Fig. 3(d). In our Monte Carlo simulation, the source intensity is changed from 1 to 80 nAm. Such source intensity corresponds to the SNR approximately between 0.05 and 5 for the three-source case, and this is the SNR range encountered in real-life MEG measurements.

A plots of the A-prime metric versus the source intensity for four different number of sources are shown in Fig. 4. As shown in this figure, the general tendency is that when the number of sources increases, the A-prime metric decreases. However, we can also see that, in the limit of strong source intensity, the A-prime metric becomes close to one for all four cases. Conversely, in the limit of low SNR, the A-prime metric becomes close to zero for all four cases. We also computed the A-prime metric for four different types of sensor systems in Fig. 2. Here, the number of sources was fixed at five. The results are shown in Fig. 5. These results
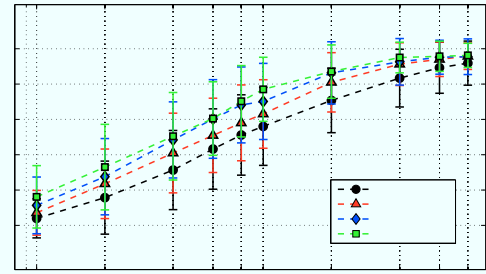

Fig. 5. A-prime metric versus source intensity for four different types of sensor systems shown in Fig. 2. The number of sources was fixed at five.

express how the sensor-array ability to detect five sources changes according to the number of sensors.
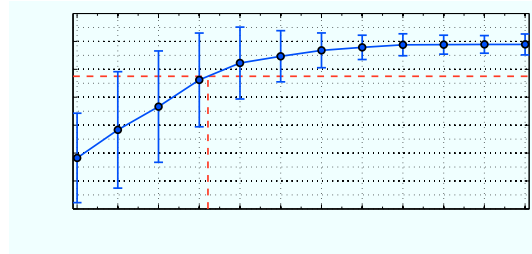

Fig. 6. Plot of the A-prime metric with respect to the inter-source distance. The 160 sensor system with a 13 cm sphere radius was assumed and the source intensity was set at 70 nAm.

C. Spatial Resolution

We next assessed the spatial resolution of four types of sensor systems in Fig. 2. The plot of the A-prime metric with respect to the inter-source distance is shown in Fig. 6 in which the 160 sensor system with a 13 cm sphere radius was assumed and the source intensity was set at 70 nAm. The figure shows that the A-prime metric decreases when the inter-source distance of the two sources decreases. According to this plot, the spatial resolution can be determined approximately to be 2.1 cm in this case with $\alpha = 0.75$.

We repeated exactly the same procedure changing the source intensity from 4 to 400 nAm, and obtained the plots of the resolution with respect to the source intensity. The resultant plots for four types of sensor systems are shown in Fig. 7. In this figure, we also plot the results of sensor arrays having the same sensor numbers on a sphere of a 10-cm radius. The results show that the spatial resolution becomes high, when the source intensity becomes strong. (i.e., when SNR becomes high.) Also, sensor systems with larger number of sensors have higher spatial resolution. The difference of the spatial resolution for different number of sensors becomes large in a low SNR, and small in a high SNR. The spatial resolution in a very high SNR situation may be referred to as the asymptotic resolution, and the resolution plot shows that the asymptotic resolution does not depend on the number of sensors, and it depends only on the size
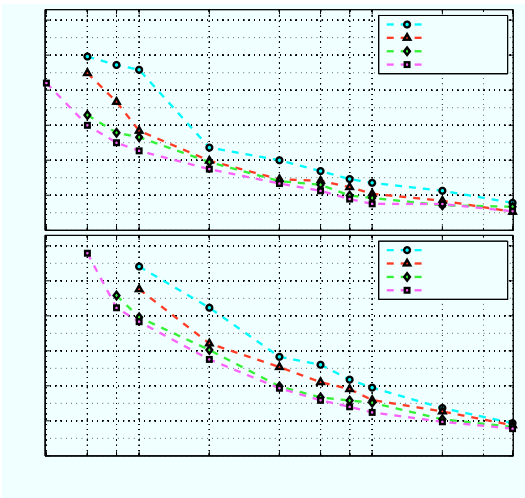
Fig. 7. Spatial resolution with respect to source intensity for the 80, 160, 320, 614 sensor systems. The sensor-aligned sphere had a 10 cm radius (upper panel) and 13 cm radius (lower panel). The sensor noise was assumed to have a standard deviation of 50 fT.

of the sphere on which sensors are aligned. The asymptotic resolution is approximately 1 cm for a system with a 13-cm sphere, and it is close to 0.5 cm for a system with a 10-cm sphere.

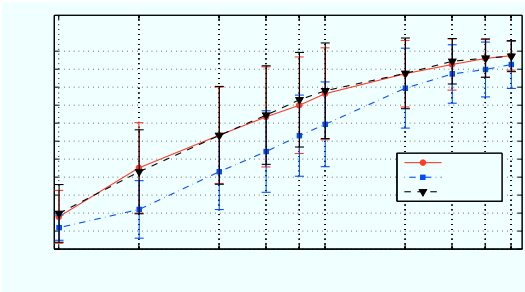*D. Performance Assessments of Existing Neuromagnetic Sensor Systems*

Fig. 8. A-prime metric for MEG vision^{TM} and Elekta-Neuromag TRIUX^{TM}. The plots labeled "Y", "EL-PG", and "EL-PG+M", respectively, indicate the plot for MEGvision, that for TRIUX in which only the planar gradiometer sensors are used, and that for TRIUX in which all sensors are used.

We computed the performance metrics of two types of existing neuromagnetic sensor systems. One is MEGvision^{TM} (Yokogawa Electric Corporation, Tokyo, Japan), which has 160 sensors aligned on a helmet-shaped surface[8]. The sensors are first-order axial gradiometers with a 5 cm baseline. The other is Elekta-Neuromag TRIUX^{TM} (Elekta Corporate, Stockholm, Sweden), which has total 306 sensors consisting of 204 planer gradiometers with a baseline of 1.4 cm and 102 magnetometers.

The plots of the A-prime metric are shown in Fig. 8, and plots of spatial resolution are in Fig. 9. In these figures, The plot labeled "Y" indicates the results from MEGvision^{TM}.

The plot labeled "EL-PG" indicates the results from TRIUX in which only the planar gradiometer sensors are used, and the plot labeled "EL-PG+M", indicates the plot from TRIUX in which both the planar gradiometer and magnetometer sensors are used.

Both results in Figs 8 and 9 show that the performance of MEGvision^{TM} is almost the same as Elekta-Neuromag TRIUX^{TM}. However, if only the planar-gradiometer sensors are used, the performance of TRIUX^{TM} is considerably lower than MEGvision^{TM}. We can show that this performance difference is caused primarily by a short baseline of the planar gradiometer sensors used in TRIUX^{TM}.
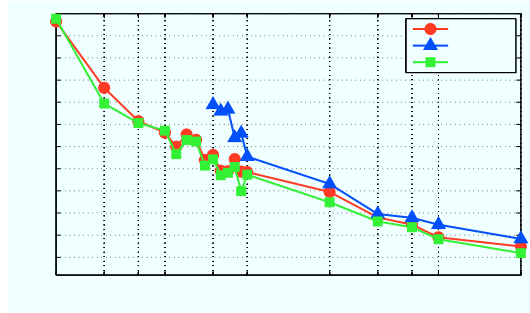

Fig. 9. Spatial resolution for MEG vision^{TM} and Elekta-Neuromag TRIUX^{TM}. The plots labeled "Y", "EL-PG", and "EL-PG+M", respectively, indicate the plot for MEGvision, that for TRIUX in which only the planar gradiometer sensors are used, and that for TRIUX in which all sensors are used.

REFERENCES

[1] M. Hämäläinen, R. Hari, R. J. Ilmoniemi, J. Knuutila, and O. V. Lounasmaa, "Magnetoencephalography-theory, instrumentation, and applications to noninvasive studies of the working human brain," *Rev. Mod. Phys.*, vol. 65, pp. 413–497, 1993.

[2] S. Baillet, J. C. Mosher, and R. M. Leahy, "Electromagnetic brain mapping," *IEEE Signal Processing Magazine*, vol. 18, pp. 14–30, 2001.

[3] K. Sekihara and S. S. Nagarajan, *Adaptive spatial filters for electromagnetic brain imaging*. Berlin, Heidelber: Springer-Verlag, 2008.

[4] J. P. Owen, D. P. Wipf, H. T. Attias, K. Sekihara, and S. S. Nagarajan, "Performance evaluation of the Champagne source reconstruction algorithm on simulated and real M/EEG data," *NeuroImage*, vol. 60, pp. 305–323, 2012.

[5] B. D. van Veen, W. van Drongelen, M. Yuchtman, and A. Suzuki, "Localization of brain electrical activity via linearly constrained minimum variance spatial filtering," *IEEE Trans. Biomed. Eng.*, vol. 44, pp. 867–880, 1997.

[6] J. Sarvas, "Basic mathematical and electromagnetic concepts of the biomagnetic inverse problem," *Phys. Med. Biol.*, vol. 32, pp. 11–22, 1987.

[7] J. Snodgrass and J. Corwin, "Pragmatics of measuring recognition memory: applications to dementia and amnesia," *J. Exp. Psychol. Gen.*, vol. 117, pp. 34–50, 1988.

[8] G. Uehara, Y. Adachi, J. Kawai, M. Shimogawara, M. Higuchi, Y. Haruta, H. Ogata, and H. Kado, "Multi-channel SQUID systems for biomagnetic measurement," *IEICE Trans. on Electronics*, vol. E86-C, pp. 43–54, 2003.